Dalton Transactions

Optically active bis(aminophenols) and their metal complexes

Journal:	*Dalton Transactions*
Manuscript ID	DT-ART-07-2023-002436.R1
Article Type:	Paper
Date Submitted by the Author:	27-Aug-2023
Complete List of Authors:	Carbonel, Halen; University of Notre Dame, Department of Chemistry and Biochemistry Mikulski, Timothy; University of Notre Dame, Department of Chemistry and Biochemistry Nugraha, Kahargyan; University of Notre Dame, Department of Chemistry and Biochemistry Johnston, James; University of Notre Dame Wang, Yichun; University of Notre Dame, Brown, Seth; University of Notre Dame, Department of Chemistry and Biochemistry

ARTICLE

Optically active bis(aminophenols) and their metal complexes

Halen Carbonel,[a] Timothy D. Mikulski,[a] Kahargyan Nugraha,[a] James Johnston,[b] Yichun Wang[b] and Seth N. Brown*[a]

Received 00th January 20xx,
Accepted 00th January 20xx

DOI: 10.1039/x0xx00000x

Optically active C_2-symmetric bis(aminophenols) based on (*R*)-2,2′-diaminobinaphthyl ($BiniqH_4$) and (*R*,*R*)-2,3-butanediyldianthranilate ($BdanH_4$) have been prepared by condensation of the diamines with 3,5-di-*tert*-butylcatechol. Group 10 bis(iminosemiquinone) complexes (*R*)-(Biniq)M (M = Pd, Pt) and (*C*,*R*,*R*)-(Bdan)Pd have been prepared by oxidatively metalating the corresponding ligands. In (*R*)-(Biniq)M, the C_2 axis passes through the approximate square plane of the bis(iminosemiquinone)metal core, while in (*C*,*R*,*R*)-(Bdan)Pd the C_2 axis is perpendicular to this plane. In the latter compound, the (*R*,*R*)-butanediyl strap binds selectively over one enantioface of the metal complex in a conformation where the methyl groups are *anti* to one another. Osmium oxo complexes with the intrinsically chiral $OsO(amidophenoxide)_2$ chromophore are obtained by metalation of $OsO(OCH_2CH_2O)_2$ with (*R*,*R*)-$BdanH_4$. Both the (*A*,*R*,*R*) and (*C*,*R*,*R*) diastereomers can be observed, with metalation in refluxing toluene selectively giving the latter isomer. The electronic structures of the complexes are illuminated by the circular dichroism spectra, in conjuction with the optical spectra and TDDFT calculations.

Introduction

Metal complexes of iminoxolene ligands show a rich chemistry by virtue of the multiple accessible redox states of the ancillary ligands (amidophenoxide/iminosemiquinone/iminoquinone).[1,2] This characteristic has been used to foster redox reactivity in complexes of both early[3] and late[4] metals that are typically redox-inactive. The redox activity of iminoxolenes is due to the presence of a molecular orbital, called the redox-active orbital (RAO), at a moderate energy. Because this energy is close to that of the d orbitals of middle transition metals, iminoxolene complexes of these metals have highly covalent π bonding,[5,6] which can result in unusual patterns of reactivity.[7]

A potential limitation of iminoxolenes as ancillary ligands is the low Lewis basicity of the neutral iminoquinones, which can result in ligand dissociation under oxidative conditions.[8] One strategy to combat this is to link multiple iminoxolenes together to take advantage of the chelate effect to inhibit ligand dissociation. The nitrogen substitutents on the iminoxolenes provide the most synthetically convenient handle for tethering, and tetradentate bis-aminophenols based on 1,2-phenylenediamine,[9] 2,2-dimethyl-1,3-propanediamine,[10] 2,2'-diaminodiphenylsulfide[11] and 1,1′-bis(*p*-aminophenyl)ferrocene[12] have been prepared and successfully metalated to form bis(iminoxolene) complexes. A tris(aminophenol) ligand based on 2,2′,2′′-triaminotri-*p*-tolylamine is also known.[13]

Less well developed have been optically active linking groups. Robust optically active aminophenol ligands would be potentially desirable for applications in asymmetric catalysis, for example in reactions catalyzed by bis(iminoxolene) complexes such as alcohol oxidation,[14] Negishi cross-coupling,[15] or olefin aziridination.[16] Furthermore, the availability of optically active iminoxolenes would allow the deployment of circular dichroism spectroscopy as a powerful spectroscopic tool to elucidate the (often complex) electronic structures of complexes with redox-active ligands.[17]

Two types of bis(iminoxolene) ligands have been prepared that afford chiral, C_2-symmetric metal complexes. The first is based on 2,2′-diaminobiphenyl, as exemplified by (^{R}Clip)Pd (Fig. 1a).[18,19] Here, the C_2 axis passes through the approximate square plane of the ligand, which must bind with the nitrogen atoms of the iminoxolenes in a cis orientation. The second is based on 1,2-ethanediyldianthranilate, exemplified by (Egan)OsO (Fig. 1b).[20] In this complex, the C_2 axis is perpendicular to the approximate plane of the two iminoxolenes, and the nitrogens are mutually trans.

These compounds have not been widely available in optically active form. The free ligand $EganH_4$ is achiral, and while 2,2′-disubstituted biphenyls are chiral, they typically racemize rapidly at or below room temperature.[21] A bis(aminophenol) derived from optically stable 6,6′-dimethyl-2,2′-diaminobiphenyl has been prepared,[22] but only metal complexes of the *N*-methyl[23] and *O*-methyl[24] derivatives have been reported. This ligand is inconvenient to use because the diamine is not commercially available and is tedious to resolve.[25] Recently, an optically active bis(aminophenol) based on commercially available 1,1′-binaphthyl-2,2′-diamine has been prepaed and complexed to copper.[26]

[a] Department of Chemistry and Biochemistry, University of Notre Dame, Notre Dame, IN 46556-5670 USA. E-mail Seth.N.Brown.114@nd.edu
[b] Department of Chemical and Biomolecular Engineering, University of Notre Dame, Notre Dame, IN 46556 USA.

† Electronic Supplementary Information (ESI) available: Crystallographic, spectroscopic, and computational details. CCDC 2281681-2281685. See DOI: 10.1039/x0xx00000x

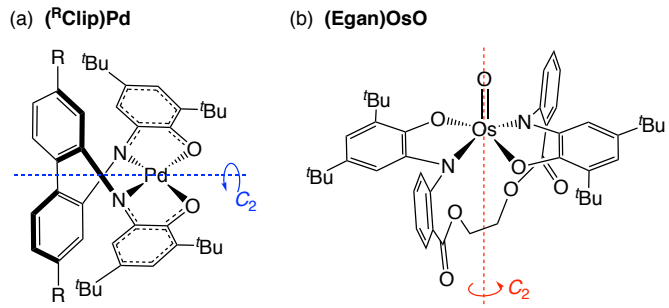

Fig. 1 C_2-symmetric complexes of bis(iminoxolene) ligands. (a) (^{R}Clip)Pd (R = H, ^{t}Bu), based on a 2,2′-diaminobiphenyl linker. (b) (Egan)OsO, based on an ethylene glycol dianthranilate linker. Dashed lines indicate the locations of the C_2 axes.

Here we report the preparation of an optically active version of the EganH_4 ligand, (*R*,*R*)-BdanH_4, using commercially available (*R*,*R*)-2,3-butanediol as starting material. Both this ligand and the bis(aminophenol) derived from (*R*)-1,1′-binaphthyl-2,2′-diamine, (*R*)-BiniqH_4, are metalated stereoselectively to give group 10 bis(iminoxolene) complexes as single stereoisomers. In contrast, both diastereomers of (Bdan)OsO can be observed, with the (*C*,*R*,*R*) diastereomer of the product isolated pure as the thermodynamic product of metalation. The chiroptical properties of the twisted bis(iminoxolene)palladium and platinum chromophores, and the intrinsically chiral bis(amidophenoxide)oxoosmium chromophore, are described and used to elucidate the electronic structures of the complexes.

Experimental

General procedures

All procedures were carried out on the benchtop without precautions to exclude air or moisture. $OsO(OCH_2CH_2O)_2$ was prepared as described by Griffith.[27] Deuterated solvents were obtained from Cambridge Isotope Laboratories. All other reagents were commercially available and used without further purification. NMR spectra were measured on a Bruker Avance DPX-400 or -500 spectrometer. Chemical shifts for ^{1}H and ^{13}C are reported in ppm downfield of TMS, with spectra referenced using the chemical shifts of the solvent residuals. Infrared spectra were recorded on a Jasco 6300 FT-IR spectrometer. UV-visible spectra were measured as CH_2Cl_2 solutions in a 1-cm quartz cell on an Agilent 8453 diode array spectrophotometer. Cyclic voltammograms were performed using an Autolab potentiostat (PGSTAT 128N), with glassy carbon working and counter electrodes and a silver/silver chloride reference electrode. The electrodes were connected to the potentiostat through electrical conduits in the drybox wall. Samples were run in CH_2Cl_2 with 0.1 M Bu_4NPF_6 as the electrolyte. Potentials were referenced to ferrocene/ferrocenium at 0 V[28] with the reference potential established by spiking the test solution with a small amount of decamethylferrocene ($E°$ = –0.565 V vs. Cp_2Fe^+/Cp_2Fe in CH_2Cl_2[29]). Circular dichroism spectra were obtained as CH_2Cl_2 solutions, using a Jasco J-1700 circular dichroism spectrophotometer, except for (*C*,*R*,*R*)-(Bdan)OsO, which was measured on a Jasco J-815 circular dichroism spectrophotometer. Elemental analyses were performed by M-H-W Labs (Phoenix, AZ, USA), Robertson Microlit (Ledgwood, NJ, USA), or Midwest Microlab (Indianapolis, IN, USA).

Syntheses

(*R*)-*N*,*N*′-Bis(2-hydroxy-3,5-di-*tert*-butylphenyl)-1,1′-binaphthyl-2,2′-diamine, (*R*)-BiniqH_4. Into a round-bottom flask are added 0.4974 g (*R*)-(+)-1,1′-binaphthyl-2,2′-diamine (1.749 mmol), 1.021 g 3,5-di-*tert*-butylcatechol (4.593 mmol, 2.6 equiv), 0.5 mL acetic acid, 10 mL benzene and a stir bar. The reaction mixture is stirred at room temperature for 24 h. The acetic acid and benzene are removed on the rotary evaporator, the residue slurried in 10 mL methanol and the solid collected by vacuum filtration and washed thoroughly with 5 × 5 mL methanol. The crude product is recrystallized by dissolving in 1 mL toluene, which is then layered with 3 mL methanol. The precipitate is collected by vacuum filtration after 1 d and washed thoroughly with 5 × 5 mL methanol, to afford 0.9659 g (80%) BiniqH_4. ^{1}H NMR (C_6D_6): δ 1.26 (s, 18H, ^{t}Bu), 1.62 (s, 18H, ^{t}Bu), 4.75 (s, 2H, NH), 6.55 (s, 2H, OH), 6.95 (d, 2 Hz, 2H, hydroxyaniline H-6), 7.10 (m, 4H, binaphthyl H-6,6′,7,7′), 7.11 (d, 9 Hz, 2H, binaphthyl H-3,3′), 7.33 (dd, 8, 1 Hz, 2H, binaphthyl H-8,8′), 7.42 (d, 2 Hz, 2H, hydroxyaniline H-4), 7.56 (d, 9 Hz, 2H, binaphthyl H-4,4′), (dd, 8, 1 Hz, 2H, binaphthyl H-5,5′). ^{13}C{^{1}H} NMR (C_6D_6): δ 29.89 (C[*C*H$_3$]$_3$), 31.81 (C[*C*H$_3$]$_3$), 34.48 (*C*[CH$_3$]$_3$), 35.38 (*C*[CH$_3$]$_3$), 114.80, 117.00, 122.73, 123.20, 123.86, 124.26, 128.94, 129.86, 130.71, 134.12, 135.73, 142.53, 144.52, 150.60 (*C*O). IR (evapd film, cm^{-1}): 3425 (s, ν_{OH}), 3342 (m, ν_{NH}), 3055 (w), 2958 (vs), 2906 (s), 2867 (s), 1620 (s), 1595 (s), 1510 (m), 1481 (s), 1419 (s), 1382 (m), 1308 (s), 1265 (m), 1225 (s), 1201 (m), 1145 (w), 999 (w), 818 (m), 747 (m). Anal. Calcd for $C_{48}H_{56}N_2O_2$: C, 83.19; H, 8.15; N, 4.04. Found: C, 83.45, H, 8.15; N, 3.79.

(2*R*,3*R*)-2,3-Butanediyl dianthranilate. In a 100 mL round-bottom flask, 0.4380 g (*R*,*R*)-2,3-butanediol (4.86 mmol), 1.9032 g isatoic anhydride (11.7 mmol, 2.4 equiv), 30 mL chloroform and 0.4231 g 4-dimethylaminopyridine (DMAP, 3.5 mmol, 0.7 equiv) are heated at reflux for 7 d. The isatoic anhydride dissolves gradually over the course of the reaction. After cooling to room temperature, the clear solution is washed once with 100 mL 10% aqueous citric acid solution and the organic layer is collected. The aqueous layer is extracted once with 30 mL $CHCl_3$. The combined organic layers are then washed once with 100 mL water, dried over magnesium sulfate and evaporated to dryness on a rotary evaporator. The oily residue is dissolved in 10 mL methanol and left to stand in a stoppered round bottom flask overnight. The white crystals that deposit are collected by suction filtration to give 0.8642 g of the diester. The filtrate is then evaporated and the resulting oil is allowed to stand again, in 3 mL methanol, which results in a second crop with a yield of 0.2789 g for a combined yield of 1.1251 g (70%). Mp 109–111 °C. ^{1}H NMR ($CDCl_3$): δ 1.40 (d, 6.4 Hz, 6H, CH_3), 5.32 (m, 2H, OCH), 5.61 (s, 4H, NH_2), 6.68 (ddd, 8.5, 7.0, 1.5 Hz, 2H, Ar H–5), 6.69 (dd, 8.2, 1.5 Hz, 2H, Ar H–3), 7.28 (ddd, 8.3, 7.1, 1.6 Hz, 2H, Ar H–4), 7.92 (ddd, 7.8, 1.6, 0.5 Hz, 2H, Ar H-6). ^{13}C{^{1}H} NMR ($CDCl_3$): δ 16.54 (CH_3), 71.64 (O*C*HCH$_3$), 111.1, 116.7, 117.0, 131.5, 134.4, 150.6, 167.57 (C=O). IR (ATR, cm^{-1}): 3496 (m, ν_{N-H}), 3465 (m, ν_{N-H}), 3390 (m, ν_{N-H}), 3367 (m, ν_{N-H}), 3076 (w), 2988

(w), 2958 (w), 1679 (s, $\nu_{C=O}$), 1623 (s), 1585 (s), 1560 (s), 1489 (s), 1453 (m), 1444 (m), 1385 (m), 1324 (m), 1289 (m), 1233 (s), 1164 (s), 1152 (s), 1100 (s), 1073 (s), 991 (m), 859 (m), 751 (s). Optical rotation: $[\alpha]_D$ = +108° ($CHCl_3$, 0.01 g/mL). Anal. Calcd for $C_{18}H_{20}O_4N_2$: C, 65.85; H 6.14; N 8.53. Found: C, 65.99; H, 6.28; N, 8.69.

(*R*,*R*)-2,3-butanediyl-di-*N*-(2-hydroxy-3,5-di-*tert*-butylphenyl)anthranilate, $BdanH_4$. Into a 20 mL vial, 0.659 g (2*R*,3*R*)-2,3-butanediyl dianthranilate (2.0 mmol), 1.06 g 3,5-di-*tert*-butylcatechol (4.8 mmol, 2.37 equiv), 0.224 g benzoic acid (1.8 mmol, 0.9 equiv) and a stirbar are added. The vial is sealed with a Teflon-lined screwcap and placed into a 165 °C silicone oil bath. The molten mixture is heated with stirring for two days. The reaction mixture is removed from the oil, cooled to room temperature, and dissolved in CH_2Cl_2 so the material can be removed from the vial. The solvent is removed by rotary evaporation and the brown residue dissolved in minimal dichloromethane. The product is purified via column chromatography with CH_2Cl_2 as the eluent, retaining the fastest moving fractions. The dichloromethane is removed on the rotary evaporator to yield 1.079 g (73%) of the product as a yellow foam. ^{1}H NMR ($CDCl_3$): δ 1.30 (s, 9H, ^{t}Bu), 1.47 (s, 9H, ^{t}Bu), 1.50 (d, 6.3 Hz, 3H, OCHCH_3), 5.45 (m, 1H, OC*H*CH_3), 6.06 (s, 1H, OH), 6.53 (dd, 8.5, 0.8 Hz, anthranilate H–3), 6.74 (ddd, 8.1, 7.1, 1.1 Hz, 1H, anthranilate H–4), 7.04 (d, 2.4 Hz, 1H, aminophenol H–4 or H–6), 7.28 (d, 2.4 Hz, 1H, aminophenol H–6 or H–4), 7.30 (ddd, 8.5, 7.0, 1.5 Hz, 1H, anthranilate H–5), 8.05 (dd, 7.9, 1.4 Hz, 1H, anthranilate H–6), 8.88 (s, 1H, NH). ^{13}C{^{1}H} NMR ($CDCl_3$): δ 16.38 (CH_3), 29.53 (C(*C*H_3)$_3$), 31.71 (C(*C*H_3)$_3$), 34.41 (*C*(CH_3)$_3$), 35.08 (*C*(CH_3)$_3$), 71.87 (O*C*H), 111.96, 114.52, 117.33, 122.41, 122.46, 126.16, 131.39, 134.76, 135.47, 142.38, 149.35, 150.76, 167.81 (C=O). IR (ATR, cm^{-1}): 3446 (m, ν_{OH}), 3317 (m, ν_{NH}), 2958 (s), 2917 (w), 2868 (m), 1685 (s, $\nu_{C=O}$), 1601 (m), 1580 (s), 1502 (m), 1479 (m), 1453 (m), 1251 (s), 1231 (s), 1077 (m), 752 (m). Anal. Calcd for $C_{46}H_{60}N_2O_6$: C, 74.97; H, 8.21; N, 3.80. Found: C, 74.97; H, 8.24; N, 4.14.

(*R*)-[1,1′-binaphthyl-2,2′-bis-(2-oxy-3,5-di-*tert*-butylphenyliminoxolene)]palladium, (*R*)-(Biniq)Pd. A solution of 505.5 mg (*R*)-$BiniqH_4$ (0.7305 mmol) and 358.0 mg palladium(II) acetate (1.595 mmol) in 5 mL $CHCl_3$ is stirred at 60 °C for 24 hours. After evaporating the chloroform on a rotary evaporator, the dark green residue is dissolved in dichloromethane and filtered through a plug of silica gel, eluting with dichloromethane and collecting the fast-moving dark green band. The CH_2Cl_2 is removed by rotary evaporation and the dark green residue slurried in 5 mL methanol. After letting the mixture stand for 1 day, the dark green precipitate is collected by vacuum filtration and washed thoroughly with 5 × 5 mL methanol to afford 442.0 mg (77%) (*R*)-(Biniq)Pd. ^{1}H NMR ($CDCl_3$): δ 1.20 (s, 18H, ^{t}Bu), 1.47 (s, 18H, ^{t}Bu), 6.74 (s, 2H, iminoxolene H-3), 6.79 (br s, 2H, iminoxolene H-5), 7.18 (br d, 8 Hz, 2H, binaphthyl H-8,8′), 7.21 (td, 8, 1 Hz, 2H, binaphthyl H-7,7′), 7.27 (td, 8, 1 Hz, 2H, binaphthyl H-6,6′), 7.69 (d, 9 Hz, 2H, binaphthyl H-3,3′), 7.83 (d, 8 Hz, 2H, binaphthyl H-5,5′), 7.90 (d, 9 Hz, 2H, binaphthyl H-4,4′). ^{13}C{^{1}H} NMR (CD_2Cl_2): δ 29.61 (C[*C*H_3]$_3$), 31.27 (C[*C*H_3]$_3$), 34.74 (*C*[CH_3]$_3$), 35.49 (*C*[CH_3]$_3$), 115.25, 122.41 (br), 124.16 (br), 126.47, 126.93, 127.45 (br), 127.87, 128.93, 130.25, 132.30, 133.77, 140.40 (br), 142.96 (br), 146.77, 150.64, 175.73 (br, *C*O). IR (evapd film, cm^{-1}): 3067 (w), 2957 (s), 2919 (m), 2867 (m), 1581 (w), 1519 (m), 1458 (w), 1431 (w), 1386 (m), 1361 (m), 1313 (w), 1280 (w), 1266 (w), 1243 (m), 1230 (m), 1200 (m), 1182 (m), 1151 (w), 1132 (w), 1110 (m), 1078 (w), 1049 (w), 1026 (w), 999 (w), 960 (w), 936 (w), 908 (w), 859 (w), 811 (m), 768 (w), 741 (w). UV-vis-NIR (CH_2Cl_2): λ_{max} = 1031 nm (ε = 27400 L mol^{-1} cm^{-1}), 822 (sh, 11100), 600 (5000), 422 (13700), 337 (31600). Anal. Calcd for $C_{48}H_{52}N_2O_2Pd$: C, 72.48; H, 6.59; N, 3.52. Found: C, 71.88; H, 6.42; N, 3.45.

(*R*)-[1,1′-binaphthyl-2,2′-bis-(2-oxy-3,5-di-*tert*-butylphenyliminoxolene)]platinum, (*R*)-(Biniq)Pt. A mixture of 509.0 mg (*R*)-$BiniqH_4$ (0.7356 mmol), 301.4 mg potassium tetrachloroplatinate (0.7261 mmol), 136.4 mg sodium acetate (1.663 mmol), and 8 mL dimethyl formamide are stirred at 60 °C for 8 hours in a round-bottom flask that is open to the air. After cooling to room temperature, 5 mL acetonitrile is added to the reaction mixture and the solids are collected by vacuum filtration and washed with 5 × 5 mL acetonitrile. The solids are then dissolved in C_6H_6 and filtered through a plug of silica gel, eluting with C_6H_6, and collecting the fast-moving dark green band. The solvent is removed by rotary evaporation and the dark green residue slurried in 5 mL acetonitrile. After standing for 1 day, the reaction mixture is vacuum filtered and the precipitate washed thoroughly with 5 × 5 mL acetonitrile, yielding 271.8 mg (42%) (*R*)-(Biniq)Pt. ^{1}H NMR (C_6D_6): δ 1.16 (s, 18H, ^{t}Bu), 1.81 (s, 18H, ^{t}Bu), 6.80 (ddd, 8.5, 7, 1.3 Hz, 2H, binaphthyl H-7,7′), 6.96 (ddd, 8, 7, 1.1 Hz, 2H, binaphthyl H-6,6′), 7.19 (d, 2 Hz, 2H, iminoxolene H-3), 7.36 (d, 2 Hz, 2H, iminoxolene H-5), 7.37 (sl br d, 9 Hz, 2H, binaphthyl H-4,4′), 7.47 (ddd, 8, 1.3, 0.6 Hz, 2H, binaphthyl H-5,5′), 7.51 (ddt, 8, 1, 0.7 Hz, 2H, binaphthyl H-8,8′), 7.53 (d, 9 Hz, 2H, binaphthyl H-3,3′). ^{13}C{^{1}H} NMR (C_6D_6): δ 30.16 (C[CH_3]$_3$), 31.06 (C[*C*H_3]$_3$), 34.87 (*C*[CH_3]$_3$), 35.75 (*C*[CH_3]$_3$), 115.34, 121.37, 123.18, 124.44, 125.89, 127.35, 128.35, 129.42, 130.96, 131.52, 134.93, 141.09, 144.24, 145.28, 150.85, 175.86 (*C*O). IR (evapd film, cm^{-1}): 3060 (w), 2957 (s), 2922 (m), 2874 (m), 1542 (w), 1466 (w), 1387 (w), 1361 (m), 1303 (w), 1261 (w), 1240 (w), 1232 (s), 1201 (s), 1180 (s), 1149 (w), 1130 (w), 1112 (w), 1051 (w), 1028 (w), 910 (w), 862 (w), 815 (w), 768 (w), 744 (w). UV-vis-NIR (CH_2Cl_2): λ_{max} = 924 nm (ε = 37000 L mol^{-1} cm^{-1}), 704 (7300), 537 (2300), 426 (11500), 340 (sh, 10100), 315 (sh, 14000). Anal. Calcd for $C_{48}H_{52}N_2O_2Pt$: C, 65.22; H, 5.93; N, 3.52. Found: C, 64.95; H, 5.78; N, 3.07.

(*C*,*R*,*R*)-[2,3-butanediyl-bis-2-(2-oxy-3,5-di-*tert*-butylphenylimino)benzoate]palladium, (*C*,*R*,*R*)-(Bdan)Pd. Into a 20 mL vial with a screw cap are added 102.4 mg $BdanH_4$ (0.1390 mmol) and a solution of 58.5 mg palladium acetate (Strem, 0.2606 mmol, 1.87 equiv) dissolved in 3 mL chloroform. The vial is sealed with a Teflon-lined cap and placed into a 61 °C oil bath. After 2 d, the reaction mixture is cooled to room temperature and the solution loaded onto a plug of silica gel and eluted with CH_2Cl_2, collecting the fast-moving dark blue band. The solvent is removed by rotary evaporation and the dark blue residue dissolved in 3 mL methanol. After standing for 1 d, the blue crystalline precipitate is collected by suction filtration, washed with 1 mL methanol, and air-dried to give a first crop of material. A second crop is obtained by evaporating the filtrate to dryness, resuspending in 1 mL methanol, and isolating the blue crystals as described for the first crop. Total yield 77.1 mg (70%).

^{1}H NMR ($CDCl_3$): δ 0.69 (d, 6.5 Hz, 6H, CHC*H*$_3$), 0.98 (s, 18H, ^{t}Bu), 1.05 (s, 18H, ^{t}Bu), 5.05 (m, 2H, C*H*CH$_3$), 5.98 (s, 2H, iminoxolene H-3), 6.59 (br s, fwhm = 23 Hz, 2H, iminoxolene H-5), 7.44 (td, 8, 1 Hz, 2H, Ar H-5), 7.45 (d, 8 Hz, 2H, Ar H-3), 7.64 (td, 8, 1 Hz, 2H, Ar H-4), 8.00 (dd, 8, 1 Hz, 2H, Ar H-6). ^{13}C{^{1}H} NMR ($CDCl_3$): δ 15.76 (CH*C*H$_3$), 29.08 (C(*C*H$_3$)$_3$), 30.94 (C(*C*H$_3$)$_3$), 34.67 (*C*(CH$_3$)$_3$), 34.73 (*C*(CH$_3$)$_3$), 72.94 (O*C*H), 111.92, 126.25 (br), 126.72, 127.47 (br), 129.68 (br), 131.71, 132.46, 139.99 (br), 146.69, 146.93 (br), 155.26 (br), 167.11 (ester *C*=O), 175.81 (br, iminoxolene *C*O). IR (evapd film, cm^{-1}): 3068 (w), 2957 (s), 2907 (m), 2869 (m), 1714 (vs, $\nu_{C=O}$), 1596 (m), 1530 (m), 1518 (m), 1475 (m), 1447 (s), 1394 (m), 1362 (m), 1325 (s), 1281 (s), 1264 (m), 1241 (m), 1200 (m), 1177 (m), 1110 (m), 1087 (w), 1039 (w), 1001 (w), 908 (m), 852 (w), 770 (w), 745 (m), 647 (w). UV-vis-NIR (CH_2Cl_2): λ_{max} = 876 nm (ε = 34600 L mol^{-1} cm^{-1}), 670 (sh, 5000), 574 (4000), 430 (sh, 2400), 291 (sh, 22000). Anal. Calcd for $C_{46}H_{56}N_2O_6Pd$: C, 65.82; H, 6.72; N, 3.34. Found: C, 65.76; H, 6.86; N, 3.27.

(*C*,*R*,*R*)-Oxo[2,3-butanediyl-bis-2-(2-oxy-3,5-di-*tert*-butylphenylimino)benzoate]osmium, (*C*,*R*,*R*)-(Bdan)OsO. In the air, 100.5 mg $BdanH_4$ (0.1365 mmol), 60.0 mg $OsO(OCH_2CH_2O)_2$ (0.1827 mmol, 1.34 equiv), and 5.5 mL toluene are added to a 20-mL screw-cap vial. The vial is sealed with a Teflon-lined cap and heated in a silicone oil bath (bath temperature = 118 °C) for 23 h. The toluene is removed on the rotary evaporator and the dark purple residue extracted into 4 mL of 10:1 hexane:ethyl acetate. The extract is filtered through a plug of silica gel and eluted with 10:1 hexane:ethyl acetate to afford a dark brown eluate. After evaporation of the solvent, the residue is slurried with 1 mL CH_3OH and allowed to stand overnight at room temperature. The solid is collected by suction filtration on a glass frit, washed with 2 mL methanol, and air-dried 45 min to give 19.8 mg (15%) of (*C*,*R*,*R*)-(Bdan)OsO. ^{1}H NMR (CD_2Cl_2): δ 0.13 (d, 6.4 Hz, 6H, C*H*$_3$CH), 0.92 (s, 18H, ^{t}Bu), 1.11 (s, 18H, ^{t}Bu), 4.46 (q, 6.4 Hz, 2H, CH$_3$C*H*), 6.27 (d, 2 Hz, 2H, amidophenoxide Ar*H*), 6.56 (d, 2 Hz, 2H, amidophenoxide Ar*H*), 7.49 (d, 8 Hz, 2H, anthranilate H-3), 7.50 (td, 7, 1 Hz, 2H, anthranilate H-5), 7.82 (td, 8, 1.5 Hz, 2H, anthranilate H-4), 7.90 (dd, 8, 1.3 Hz, 2H, anthranilate H-6). ^{13}C{^{1}H} NMR (CD_2Cl_2): δ 14.87 (OCH*C*H$_3$), 29.60 (C[*C*H$_3$]$_3$), 31.91 (C[*C*H$_3$]$_3$), 34.59 (*C*[CH$_3$]$_3$), 34.62 (*C*[CH$_3$]$_3$), 73.06 (O*C*HCH$_3$), 110.16, 120.49, 128.82, 130.95, 131.82, 132.49, 133.76, 136.09, 146.70, 148.37, 150.89, 166.73, 167.12. IR (evapd film, cm^{-1}): 3071 (w), 2954 (s), 2905 (m), 2868 (m), 1719 (vs, $\nu_{C=O}$), 1597 (m), 1576 (w), 1478 (m), 1449 (m), 1407 (m), 1377 (w), 1362 (w), 1340 (w), 1284 (s), 1266 (m), 1241 (s), 1224 (m), 1203 (w), 1159 (w), 1128 (m), 1112 (w), 1088 (w), 1060 (w), 1042 (w), 1028 (w), 1014 (w), 999 (m), 957 (w), 937 (w), 916 (s, $\nu_{Os=O}$), 861 (m), 829 (w), 790 (w), 762 (w), 733 (s), 711 (w), 692 (w), 669 (w), 656 (w), 631 (m). UV-vis (CH_2Cl_2): λ_{max} 444 nm (ε = 13100 mol^{-1} L^{-1} cm^{-1}), 358 (18800), 333 (sh, 17000). Anal. Calcd for $C_{46}H_{56}N_2O_7Os$: C, 58.83; H, 6.01; N, 2.98. Found: C, 58.84; H, 6.02; N, 2.92.

Measurement of singlet-triplet gaps by variable-temperature NMR spectroscopy

^{1}H NMR spectra of (*R*)-(Biniq)Pd and (*C*,*R*,*R*)-(Bdan)Pd were measured on solutions in $CDCl_2CDCl_2$ in the temperature range of 236 – 293 K on a Bruker 400 MHz NMR spectrometer and 293 – 413 K on a Bruker 500 MHz NMR spectrometer. Chemical shifts were referenced to the solvent residual peak at δ 6.0 ppm. The temperature-dependence of the chemical shifts was analyzed by fitting to eqn (1) as described in the literature,[19] with δ in units of ppm, *T* in K, *A* in MHz, and Δ*E* in kcal mol^{-1}.

$$\delta_{obsd} = \delta_{dia,0\,°C} + \alpha(T - 273.15) + (63150)\frac{A}{T}(3 + e^{\Delta E/0.001987T})^{-1} \quad (1)$$

All *sp*^{2} C*H* resonances were modeled, but *sp*^{3} C*H* peaks showed negligible curvature in their δ vs. T plots and were not analyzed further. Unweighted nonlinear least-squares fitting was carried out using the Levenberg–Marquardt algorithm using the Solver routine of Microsoft Excel.[30] Global optima for these least-squares fits could be obtained in both cases (Table S1), but due to correlation between Δ*E* and the *A* values, this results in nonphysical values of the hyperfine couplings as previously described.[19] To prevent this, the spectra were modeled with the *A* value for H-5 on the iminoxolene ring (universally the largest *A* value in these compounds) constrained to be equal to the value calculated for the triplet state by DFT. Uncertainties in the fitted parameters were estimated using standard methods.[31]

Computational methods

Calculations were performed on compounds with all methyl and *tert*-butyl groups replaced by hydrogen atoms. Geometries were optimized using hybrid density functional theory (B3LYP, SDD basis set for palladium, osmium or platinum and a 6-31G* basis set for all other atoms), using the Gaussian16 suite of programs,[32] and were confirmed as minima by calculation of vibrational frequencies. Plots of calculated Kohn-Sham orbitals were generated using Gaussview (v. 6.0.16) with an isovalue of 0.04.

Table 1. Summary of crystal data.

	(*R*)-BiniqH$_4$ • CH$_3$OH • PhCH$_3$	(*R*,*R*)-2,3-C$_4$H$_8$(O$_2$CC$_6$H$_4$-2-NH$_2$)$_2$	(*C*,*R*,*R*)-(Bdan)Pd • 0.25 CH$_3$OH	(*C*,*R*,*R*)-(Bdan)OsO • CH$_3$OH	(*A*,*R*,*R*)-(Bdan)OsO • (*C*,*R*,*R*)-(Bdan)OsO
Molecular formula	$C_{56}H_{68}N_2O_3$	$C_{18}H_{20}N_2O_4$	$C_{46.25}H_{57}N_2O_{6.25}Pd$	$C_{47}H_{60}N_2O_8Os$	$C_{92}H_{112}N_4O_{14}Os_2$
Formula weight	817.12	328.36	847.34	971.17	1878.25
T/K	120(2)	120(2)	120(2)	120(2)	120(2)
Crystal system	Monoclinic	Orthorhombic	Orthorhombic	Orthorhombic	Monoclinic
Space group	$P2_1$	$P2_12_12$	$P2_12_12_1$	$P2_12_12_1$	$P2_1$
λ/Å	0.71073 (Mo Kα)	1.54178 (Cu Kα)	0.71073 (Mo Kα)	1.54178 (Cu Kα)	1.54178 (Cu Kα)
Total data collected	82110	29865	287291	85065	93554
No. of indep reflns.	9921	3283	22201	17517	16870
R_{int}	0.0687	0.0259	0.1088	0.0528	0.0340
Obsd refls [$I > 2\sigma(I)$]	7691	3250	19585	16604	15998
a/Å	15.1059(14)	13.6305(5)	14.7503(5)	12.7929(3)	12.7971(4)
b/Å	9.4304(9)	9.5069(3)	19.4021(6)	18.4722(4)	13.0573(4)
c/Å	17.6428(16)	12.8227(4)	31.1892(11)	37.6599(7)	25.7200(8)
α/°	90	90	90	90	90
β/°	102.041(2)	90	90	90	95.8873(15)
γ/°	90	90	90	90	90
V/Å^3	2458.0(4)	1661.61(10)	8925.9(5)	8899.5(3)	4275.0(2)
Z	2	4	8	8	2
μ/mm^{-1}	0.067	0.769	0.463	5.847	6.049
Crystal size/mm	0.43 × 0.19 × 0.13	0.25 × 0.14 × 0.05	0.16 × 0.08 × 0.07	0.08 × 0.08 × 0.03	0.12 × 0.08 × 0.08
No. refined params	630	297	1422	1049	1009
*R*1, *wR*2 [$I > 2\sigma(I)$]	*R*1 = 0.0888	*R*1 = 0.0250	*R*1 = 0.0384	*R*1 = 0.0254	*R*1 = 0.0195
	*wR*2 = 0.1977	*wR*2 = 0.0743	*wR*2 = 0.0661	*wR*2 = 0.0575	*wR*2 = 0.0471
*R*1, *wR*2 [all data]	*R*1 = 0.1268	*R*1 = 0.0252	*R*1 = 0.0495	*R*1 = 0.0279	*R*1 = 0.0213
	*wR*2 = 0.2183	*wR*2 = 0.0744	*wR*2 = 0.0693	*wR*2 = 0.0586	*wR*2 = 0.0479
Goodness of fit	1.239	1.050	1.070	1.020	1.046

X-ray crystallography

Crystals of (*R*,*R*)-2,3-C$_4$H$_8$(O$_2$CC$_6$H$_4$-2-NH$_2$)$_2$, (*C*,*R*,*R*)-(Bdan)OsO • CH$_3$OH and (*C*,*R*,*R*)-(Bdan)Pd • 0.25 CH$_3$OH deposited from methanol solutions of the respective complexes. The quasiracemate (*C*,*R*,*R*)-(Bdan)OsO • (*A*,*R*,*R*)-(Bdan)OsO crystallized from a hexane solution of a reaction mixture formed by metalation of BdanH$_4$ with OsO(OCH$_2$CH$_2$O)$_2$ in benzene at 80 °C. Crystals of (*R*)-BiniqH$_4$ • CH$_3$OH • PhCH$_3$ were grown by vapor diffusion of methanol into a toluene solution of the ligand.

Crystals were placed in inert oil before transferring to the N$_2$ cold stream of a Bruker Apex II CCD diffractometer. Data were reduced, correcting for absorption, using the program SADABS. Calculations used SHELXTL (Bruker AXS),[33] with scattering factors and anomalous dispersion terms taken from the literature.[34]

In (*R*)-BiniqH$_4$ • CH$_3$OH • PhCH$_3$, the toluene of solvation was somewhat disordered and was refined by restraining the ring carbon atoms to have similar thermal displacement parameters using the SIMU command. In (*C*,*R*,*R*)-(Bdan)Pd • 0.25 CH$_3$OH, there were two inequivalent complexes in the asymmetric unit. One *tert*-butyl group (centered at C28) was observed in two different orientations, which were refined with opposite carbon atoms constrained to have the same displacement parameters while the occupancy of the two orientations was allowed to refine. In this structure, one methanol of solvation was found on the difference map; its occupancy was fixed at 50%, in agreement with NMR measurements of the crystals, which indicated that there were approximately 0.25 mol methanol per mol (Bdan)Pd. The carbon and oxygen of this lattice solvent were refined isotropically (all other nonhydrogen atoms in the structures were refined anisotropically). In (*R*)-BiniqH$_4$ • CH$_3$OH • PhCH$_3$, (*R*,*R*)-2,3-C$_4$H$_8$(O$_2$CC$_6$H$_4$-2-NH$_2$)$_2$, and (*C*,*R*,*R*)-(Bdan)Pd • 0.25 CH$_3$OH, hydrogen atoms were found on difference Fourier maps and refined isotropically, with the exception of those on lattice solvents, on methyl groups and on O1 in BiniqH$_4$, and on the disordered *tert*-butyl group in (Bdan)Pd. These latter hydrogens, as well as all the hydrogens in the two osmium structures, were placed in calculated positions and refined with their isotropic thermal parameters tied to the atom they are attached to (1.5× for CH$_3$ groups, 1.2× for all others). Further details about the structures are in Tables 1 and 2.

Table 2. Selected bond distances, angles, and metrical oxidation states of iminoxolene ligands of structurally characterized compounds. Values given are the average of chemically equivalent measurements (averaged over the noncrystallographic twofold axes in all structures and over the optically pure and quasiracemic crystals for (*C*,*R*,*R*)-(Bdan)OsO). DFT MOS calculations use ligands in which *tert*-butyl groups are replaced by hydrogen.

	(*C*,*R*,*R*)-(Bdan)Pd	(*C*,*R*,*R*)-(Bdan)OsO	(*A*,*R*,*R*)-(Bdan)OsO	(Egan)OsO[20]
Bond distances / Å				
M–O1	1.986(12)	1.941(6)	1.934(11)	1.929(5)
M–N1	1.968(14)	1.936(4)	1.926(10)	1.9286(16)
Os=O		1.705(4)	1.705(3)	1.6951(9)
O1–C11	1.311(8)	1.371(8)	1.370(6)	1.3674(14)
N1–C12	1.354(8)	1.407(10)	1.424(12)	1.406(3)
C11–C12	1.433(6)	1.401(9)	1.391(11)	1.386(3)
C12–C13	1.417(6)	1.382(9)	1.392(11)	1.389(3)
C13–C14	1.369(7)	1.398(8)	1.397(8)	1.3881(17)
C14–C15	1.424(10)	1.399(8)	1.403(12)	1.401(2)
C15–C16	1.379(6)	1.403(11)	1.404(18)	1.3938(17)
C11–C16	1.431(10)	1.391(11)	1.393(14)	1.397(3)
Metrical Oxidation State (MOS)[35]	–1.09(4)	–2.06(7)	–2.11(13)	–1.98(12)
MOS from DFT calculations	–1.15(6)	–1.95(7)	–1.93(7)	–1.95(7)
Bond angles / °				
O1–M–O2	177(2)	144.6(17)	147.75(17)	142.66(4)
N1–M–N2	172(4)	140.1(18)	135.15(16)	138.69(4)
O1–M–N1	81.59(15)	80.8(4)	80.9(3)	80.66(17)
O1–M–N2	98(3)	87.3(10)	86.9(11)	86.4(5)
O–Os–O1		107.7(8)	106.1(4)	108.67(16)
O–Os–N1		109.9(9)	112.4(3)	110.66(6)

Results and Discussion

Synthesis and characterization of optically active bis-aminophenols. The bis-aminophenol (*R*)-*N*,*N*′-bis-(2-hydroxy-3,5-di-*tert*-butylphenyl)-1,1′-binaphthyl-2,2′-diamine, $BiniqH_4$, is prepared in good yield by condensation of 3,5-di-*tert*-butylcatechol with (*R*)-1,1′-binaphthyl-2,2′-diamine in the presence of acetic acid (eqn (2)). The reaction appears to be faster when carried out in benzene, compared to the reported preparation in hexane.[26] NMR spectra confirm the C_2 symmetry of the product and both O-H and N-H stretches are observed by IR spectroscopy. The solid-state structure of (*R*)-$BiniqH_4$, as determined by single crystal X-ray diffraction (Table 1), shows the ligand in a conformation roughly appropriate for square planar coordination (Fig. 2). The presence of a lattice methanol accepting hydrogen bonds from the two phenolic O-H groups may play a role in holding it in this conformation (see ESI, Fig. S1). The 105.7° dihedral angle between the naphthalene rings may be compared with the value of 99.1° in racemic $BiniqH_4$ (as the acetonitrile solvate)[26] and with angles in the parent diamine of 80.3° and 83.8° in the crystalline racemate[36] and 106.6° in the optically active diamine.[37] Calculations have shown that the potential energy surface for binaphthyl rotation is extremely flat in the range of $\theta = 60 - 120°$.[38]

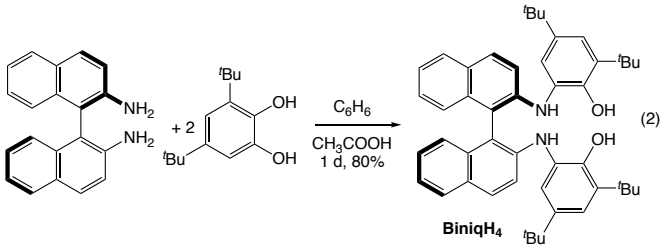

(2)

The butanediol-derived bis-aminophenol (*R*,*R*)-2,3-butanediyl-di-*N*-(2-hydroxy-3,5-di-*tert*-butylphenyl)anthranilate, $BdanH_4$, is prepared analogously to its achiral ethylene glycol analogue $EganH_4$ (Scheme 1).[20] Anthraniloylation of (*R*,*R*)-2,3-butanediol by isatoic anhydride,[39] catalyzed by 4-dimethylaminopyridine (DMAP), occurs in good yield but requires longer reaction times than does the reaction of ethylene glycol. Benzoic acid-catalyzed condensation of the dianiline with 3,5-di-*tert*-butylcatechol in the melt affords the ligand (*R*,*R*)-$BdanH_4$. Analysis of the ^{1}H NMR signals of the $A_3BB'A'_3$ system of the $CH_3CHCHCH_3$ backbone of the diesters gives $J_{BB'}$ = 4.6 Hz for the dianthranilate (Fig. S8) and $J_{BB'}$ = 5.2 Hz for $BdanH_4$ (Fig. S10). These coupling constants suggest a mixture of conformations in which H-2 and H-3 are *gauche* and ones in which they are *anti*. The two independent molecules in solid (*R*,*R*)-2,3-butanediol dianthranilate (Fig. S2) both have conformations with *anti* esters and *gauche* 2,3-hydrogens (dihedral angles = 54.5° and 56.4° in the two molecules).

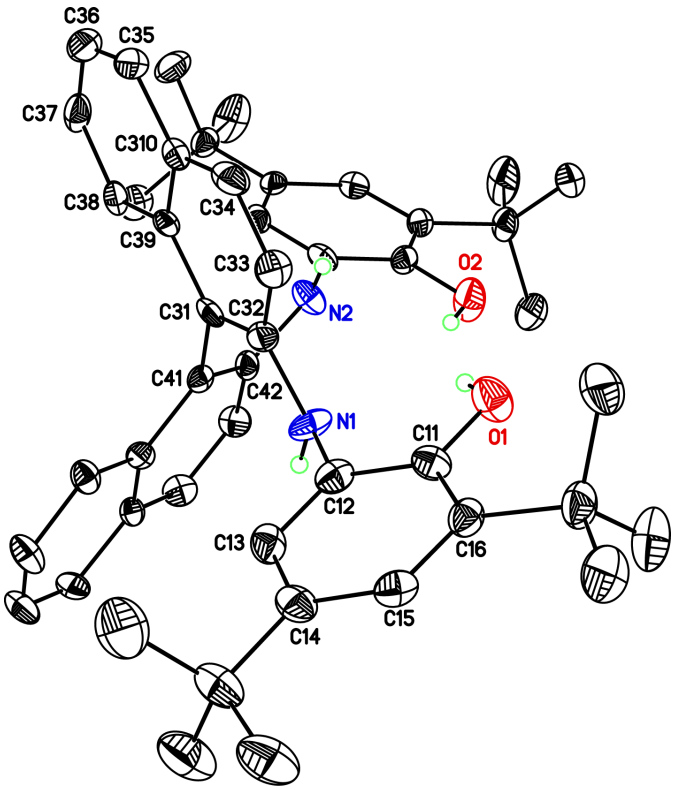

Fig. 2 Thermal ellipsoid plot of $BiniqH_4 \bullet CH_3OH \bullet PhCH_3$ (50% ellipsoids). Lattice solvent and hydrogens bonded to carbon are omitted for clarity.

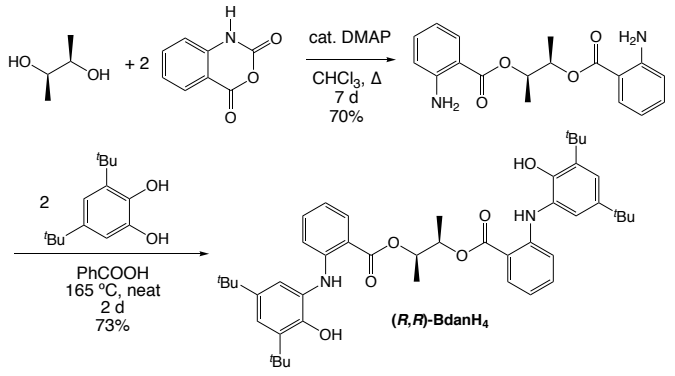

Scheme 1. Preparation of (*R*,*R*)-$BdanH_4$.

Synthesis of bis-iminoxolene-palladium and -platinum complexes. Palladium and platinum complexes of (*R*)-Biniq are prepared analogously to their ^{t}BuClip analogues.[19] Two equivalents of palladium acetate react with (*R*)-$BiniqH_4$ to give (*R*)-(Biniq)Pd and an equivalent of elemental palladium (eqn (3)). Unlike the reaction of ^{t}BuClipH_4, which occurs at room temperature, $BiniqH_4$ requires heating to 60 °C to be metalated at a reasonable rate. Metalation with platinum is achieved by heating the ligand with K_2PtCl_4 and sodium acetate as a base in DMF in the air (eqn (4)). While we were unable to obtain solid-state structures of these compounds, DFT calculations indicate that the *R* configuration of the Biniq ligand induces a *M* sense of helicity between the iminoxolene planes, consistent with previously measured structures of 2,2′-biaryl-bridged bis(iminoxolenes) of group 10[18,19] and group 8[5] compounds.

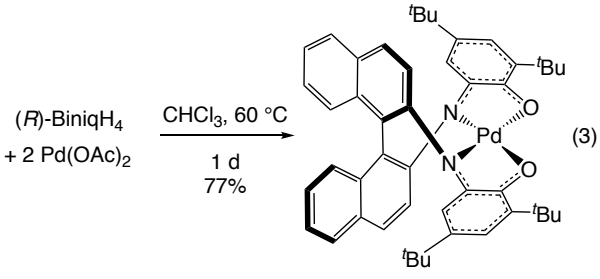

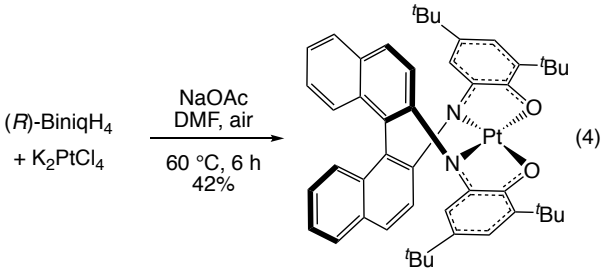

The bis(aminophenol) (*R*,*R*)-$BdanH_4$ is also metalated upon heating with palladium acetate, although the reaction is slower than with (*R*)-$BiniqH_4$ (eqn (5)). *In situ* monitoring shows that the reaction is initially quantitative for formation of the product, but that a small amount of an unidentified impurity is formed at the end of the reaction if it is carried out with excess palladium. This impurity could not be separated from the major product, so preparative reactions were conducted with less than 2 mol Pd per mol $BdanH_4$. Under these conditions, the product is formed cleanly and can be isolated in good yield and high purity after filtration through silica gel (to remove Pd black) and crystallization from methanol. Attempts to metalate $BdanH_4$ with platinum were unsuccessful.

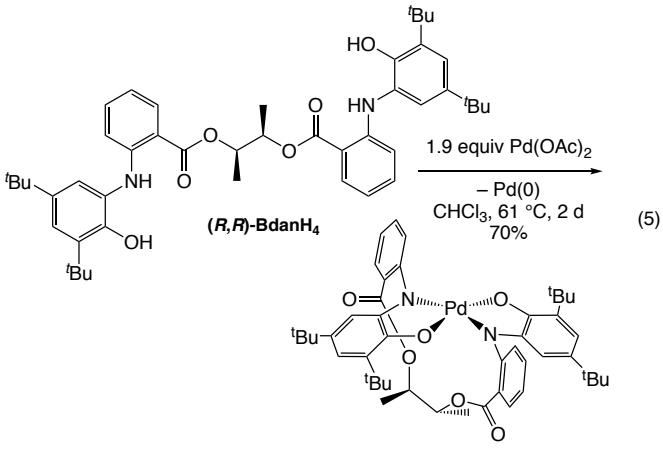

Because the two faces of a trans Pd(iminoxolene)$_2$ complex are prochiral, palladation of (*R*,*R*)-$BdanH_4$ can potentially produce two diastereomeric complexes. The ^{1}H and ^{13}C{^{1}H} NMR spectra are consistent with formation of only a single diastereomer, and analysis of the $A_3BB'A'_3$ system of the 2,3-butanediyl bridge gives $J_{BB'}$ = 1.2 Hz (Fig. S14), indicating a rigid conformation where the 2- and 3-hydrogens have a *gauche* relationship. X-ray crystallography reveals that the compound is the (*C*,*R*,*R*) diastereomer (Fig. 3), with the *C* designation based on an *SP*-4

geometry about palladium, treating its coordination sphere as slightly pyramidalized with the apex of the pyramid pointed away from the butanediyl bridge.[40] The observed conformation of the 2,3-butanediyl bridge, with *anti* methyl groups, is consistent with the NMR data in solution, and the C2–C3 bond is roughly parallel to the N–N axis of the Pd coordination sphere, similar to that seen in ethanediyl-bridged (Egan)OsO.[20] Binding of the chiral ligand induces a slight twist between the iminoxolene planes (average C–O–Pd–N torsion angles of –167.6° in the solid state, –168.4° by DFT), with a *P* sense of helical chirality relating the iminoxolene planes. Metalation is highly stereoselective, and the observed diastereomer is the more stable according to DFT calculations (computed to be favored by 2.0 kcal mol^{-1} in free energy).

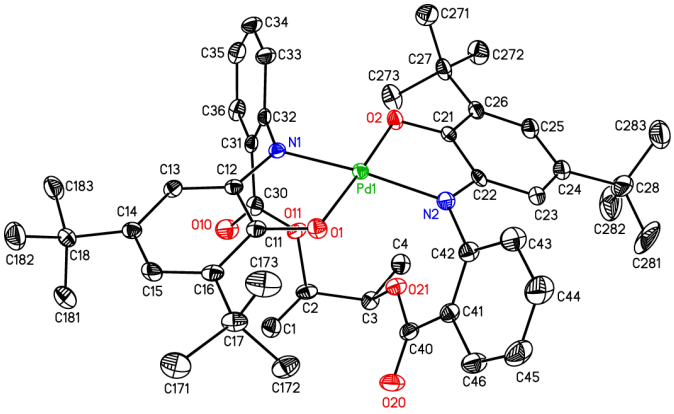

Fig. 3 Thermal ellipsoid plot of one of the two crystallographically independent metal complexes in (*C*,*R*,*R*)-(Bdan)Pd • CH_3OH, with hydrogen atoms omitted for clarity.

NMR and electrochemical characterization of bis(iminoxolene)palladium and -platinum complexes. All of the group 10 complexes show diamagnetic, C_2-symmetric NMR spectra. As seen in other palladium bis(iminoxolene) complexes,[19] some of the resonances in the room temperature ^{1}H NMR spectrum of (*R*)-(Biniq)Pd are perceptibly broadened, with chemical shifts that have a noticeable nonlinear temperature dependence (Fig. 4a). This is attributed to a singlet-triplet equilibrium, and analysis of the temperature dependence of the signals (Fig. 4b) as previously described gives a singlet-triplet gap of 1458(9) cm^{-1}, smaller than the gap seen in (^{t}BuClip)Pd (1940 cm^{-1}).[19] The ^{1}H NMR chemical shifts of (Bdan)Pd show also show a temperature dependence consistent with a singlet-triplet equilibrium (Figs. S34, S36), with a somewhat larger singlet-triplet gap of 1729(4) cm^{-1}. Because of stronger metal-ligand π bonding, the Pt complex does not show appreciable broadening or shifting in its NMR spectra.

Reported group 10 bis(iminoxolene) complexes invariably show cyclic voltammograms with four reversible redox waves corresponding to interconversions of the five redox states ranging from –2 to +2. (*C*,*R*,*R*)-(Bdan)Pd shows exactly this behavior in its cyclic voltammogram (Fig. S32), at typical potentials for this class of compound (Table 3). The Biniq complexes each show two reversible reductions (Table 3, Fig. 5). The similarity of the reduction potentials of (Biniq)Pd to those

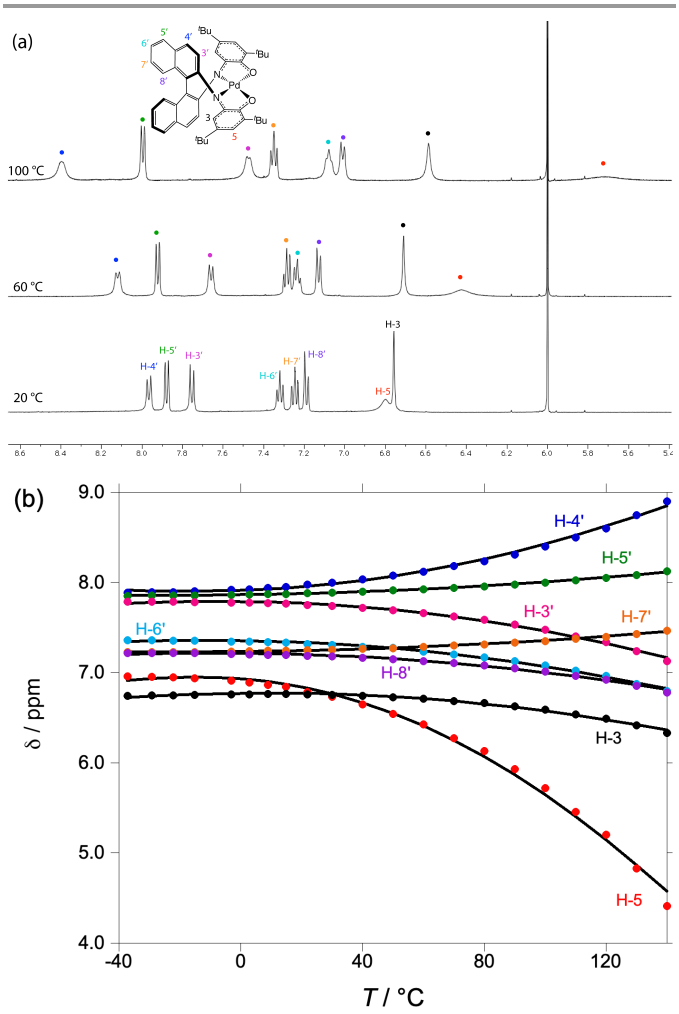

Fig. 4 (a) Downfield region of the ^{1}H NMR spectra of (*R*)-(Biniq)Pd ($CDCl_2CDCl_2$). The peak at δ 6.0 ppm is the solvent residual. (b) Temperature-dependence of chemical shifts of *sp*^{2} *CH* peaks in (*R*)-(Biniq)Pd. Solid lines are the fits to eq 1.

Table 3. Experimental and calculated (TDDFT) absorption maxima (nm) and *E*° (vs. Cp_2Fe^+/Cp_2Fe) for the $L_2M^{0/-}$ and $^{-/2-}$ couples for the for bis(iminoxolene)palladium and -platinum complexes. Calculations are performed on structures where all *tert*-butyl groups in the ligands are replaced with hydrogen.

Compound	λ_{max} / nm exptl	λ_{max} / nm calc	*E*° / V, $L_2M^{0/-}$	*E*° / V, $L_2M^{-/2-}$	Ref.
(^{H}ap)$_2$Pd[a]	875	878	–0.99	–1.40	41a
(Snip)$_2$Pd[b]	865		–1.19	–1.67	19
(*C*,*R*,*R*)-(Bdan)Pd	876	840	–1.12	–1.67	This work
(Clip)Pd[c]	961	915	–0.80	–1.27	18
(^{t}BuClip)Pd[d]	963		–0.95	–1.43	19
(Biniq)Pd	1031	1027	–0.79	–1.27	This work
(^{H}ap)$_2$Pt[a]	813	737	–1.07	–1.64	41b
(Snip)$_2$Pt[b]	796		–1.24	–1.91	19
(^{t}BuClip)Pt[d]	861	786	–1.03	–1.65	19
(Biniq)Pt	924	866	–0.84	–1.47	This work

[a] ^{H}ap = 3,5-^{t}Bu$_2$-2-O-C_6H_2NPh. [b] Snip = 3,5-^{t}Bu$_2$-2-O-C_6H_2N(C_6H_3-3,5-^{t}Bu$_2$). [c] Clip = 1,1'-(C_6H_4-2-N[C_6H_2-3,5-^{t}Bu$_2$-2-O])$_2$. [d] ^{t}BuClip = 4,4'-^{t}Bu$_2$-1,1'-(C_6H_3-2-N[C_6H_2-3,5-^{t}Bu$_2$-2-O])$_2$.

of the 2,2′-biphenyl bridged analogue (Clip)Pd[18] indicate that the biphenyl and binaphthyl groups are similar in their electron-donating ability, while the presence of the 4,4′-*tert*-butyl groups in (^{t}BuClip)M shifts the reduction waves cathodically by 160-190 mV.[19]

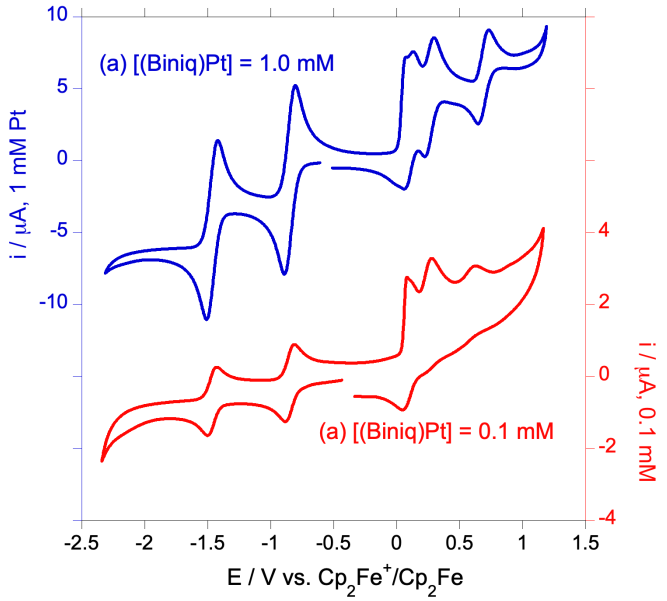

Fig. 5 Cyclic voltammograms (CH_2Cl_2, 0.1 M Bu_4NPF_6, 20 mV s^{-1}) of (a) 1.0 mM (Biniq)Pt and (b) 0.1 mM (Biniq)Pt.

The oxidation waves of the (Biniq)M complexes do not conform to the usual behavior of bis(iminoxolene)palladium and -platinum complexes. For example, (Biniq)Pt shows four discernible oxidation waves rather than the usual two (Fig. 5a). This behavior is tentatively ascribed to formation of dimeric species upon oxidation, which is consistent with the oxidation waves changing in appearance as the concentration of the metal complex varies (Fig. 5b). The palladium complex is qualitatively similar, though the waves are not as well resolved (Fig. S33). While such oxidative dimerization has not been previously observed for bis(iminoxolene) complexes, it is well documented for the isoelectronic bis(benzenediimine) complexes, for which metal-metal bonded dimeric dications have been characterized crystallogaphically.[42]

Optical and CD spectroscopy and electronic structure of bis(iminoxolene)palladium and -platinum complexes. Optical spectra of square planar bis(iminoxolene) complexes of group 10 metals are dominated by intense, relatively narrow peaks in the red or near-IR. This feature is due to a transition between the lower-lying ligand-centered RAO combination (A_u in the C_{2h} symmetry of a simple *trans*-M(iminoxolene)$_2$ complex) and the higher-lying B_g combination, whose energy is raised due to a π* interaction with a metal d_π orbital.[19,41] Optical spectra of (*R*)-(Biniq)Pd and -Pt and (*C*,*R*,*R*)-(Bdan)Pt (Fig. 6) show the expected intense bands in the near-IR. The trends in λ_{max}, with Pt compounds absorbing at shorter wavelengths than Pd compounds and cis biaryl-bridged compounds at longer wavelengths than trans compounds, are qualitatively in line with literature precedent.[19]

Quantitatively, it is noteworthy that the absorptions of the Biniq compounds are red-shifted by about 50 nm compared to those of their 2,2'-biphenyl-bridged analogues (Table 3). This is an appreciable perturbation, compared to the ~100 nm red-shift of the biphenyl-bridged compounds relative to planar analogues, and makes the optical absorptions of the Biniq complexes the most red-shifted of any platinum or palladium bis(iminoxolene) complex. A previous study of the 2,2'-biphenyl-bridged compounds concluded that the red shift in their absorptions was due to a decrease in the exchange interaction K_{12} in these compounds, ascribed to the twisting of the MN_2O_2 core in the biphenyl-bridged compounds.[19] This analysis does not appear consistent with the observations made here. The value of K_{12} can be determined from the difference between the optical absorption energy and the singlet-triplet gap, which gives a value of 4120 cm^{-1} for (Biniq)Pd, not appreciably different from

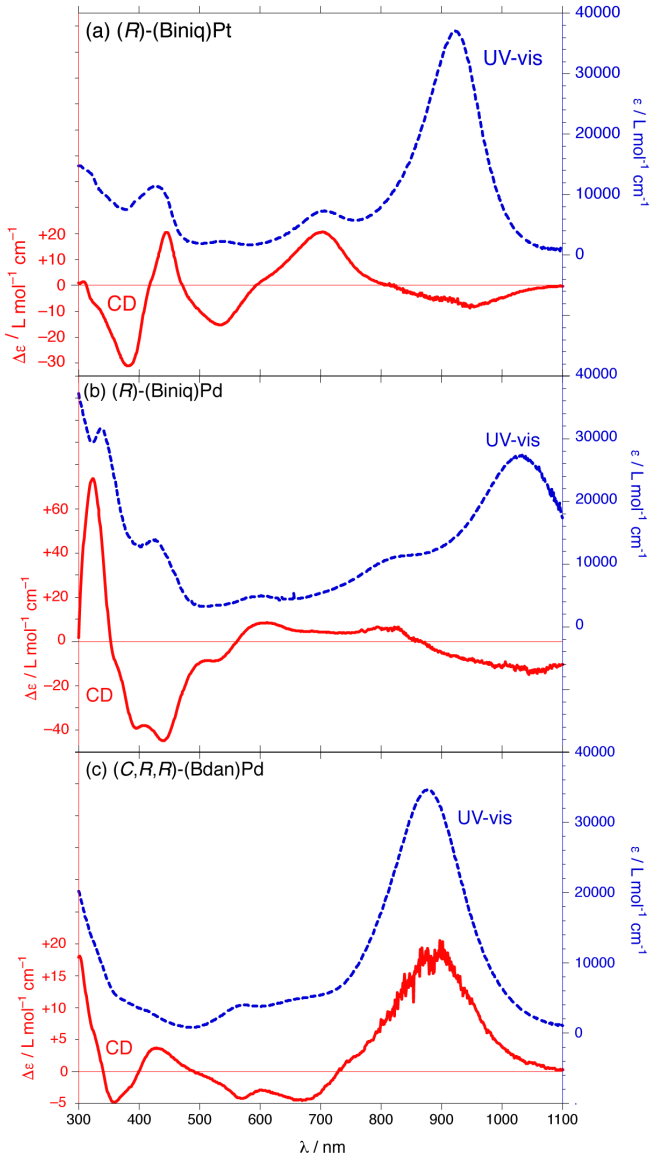

Fig. 6 Optical (blue dashed lines, right axes) and circular dichroism (red solid lines, left axes) spectra in CH_2Cl_2 of (a) (*R*)-(Biniq)Pt, (b) (*R*)-(Biniq)Pd and (c) (*C*,*R*,*R*)-(Bdan)Pd.

K_{12} = 4220 cm^{-1} for (^{t}BuClip)Pd. The twisting of the core also does not appear to be germane to the observed optical spectra. While we have not been able to determine the solid state structure of (Biniq)Pd or (Biniq)Pt, their DFT-optimized structures have cores that are essentially superimposable on those calculated for (Clip)Pd and (Clip)Pt (Figs. S37–S38, Table S6). Conversely, (*C*,*R*,*R*)-(Bdan)Pd has a noticeably twisted core, but its optical absorption is not shifted compared to planar analogues (Table 3). While we do not have a good qualitative explanation for the highly red-shifted absorbances of the Biniq complexes, the (^{H}ap)$_2$ < Clip < Biniq progressions in λ_{max} for both the Pt and Pd complexes are well reproduced by TDDFT (Table 3).

Circular dichroism spectra of the three complexes all show features corresponding to the intense long-wavelength bands (Fig. 6). These CD bands are negative for the two Biniq compounds and positive for (*C*,*R*,*R*)-(Bdan)Pd. This correlates with the twisting of the two iminoxolene planes relative to one another, with the planes in the Biniq compounds forming a *M* helix and the Bdan complex a *P* helix.

The CD spectra also show significant features at shorter wavelengths. The optical spectra of bis(iminoxolene) group 10 complexes are indeed quite complex in the visible region, but these features, which are weaker than the near-IR bands but still moderately intense (ε = 2000 – 14000 L mol^{-1} cm^{-1}), have hitherto not been interpreted. With the aid of the additional information afforded by the CD spectra, the predictions of TDDFT can be correlated with increased confidence to the experimental data, allowing one to expand the description of the bonding in these complexes beyond just the HOMO and LUMO.

The bonding in (Bdan)Pd appears to be quite similar to a typical planar trans-bis(iminoxolene) complex (Fig. 7). The HOMO–1 and HOMO–2 are principally the two combinations of the out-of-phase lone pair combinations on the ligands (the so-called subjacent orbitals or SJOs). The metal d_{z^2} orbital is the main contributor to the HOMO–3, but the pyramidalization at Pd allows this to mix with the ligand π orbitals, which gives the transition between it and the LUMO some intensity. The LUMO+1 is the σ* orbital, principally Pd $d_{x^2-y^2}$.

In the Biniq complexes, the bonding is similar (Fig. 8), except that the binaphthyl π* orbitals are now high enough in energy to be relevant to the optical spectra, with the *B* orbital in its own right as the HOMO–3 and the *A* orbital mixing with the *A*-symmetry SJO combination at higher energy (HOMO–1 for Pd, HOMO–2 for Pt). Strikingly, the CD spectra of the Pd and Pt congeners are not especially similar in appearance. This is principally due to the pronounced blue shift of the HOMO→LUMO+1 transition in the Pt complex, which changes the energy order of the observed transitions.

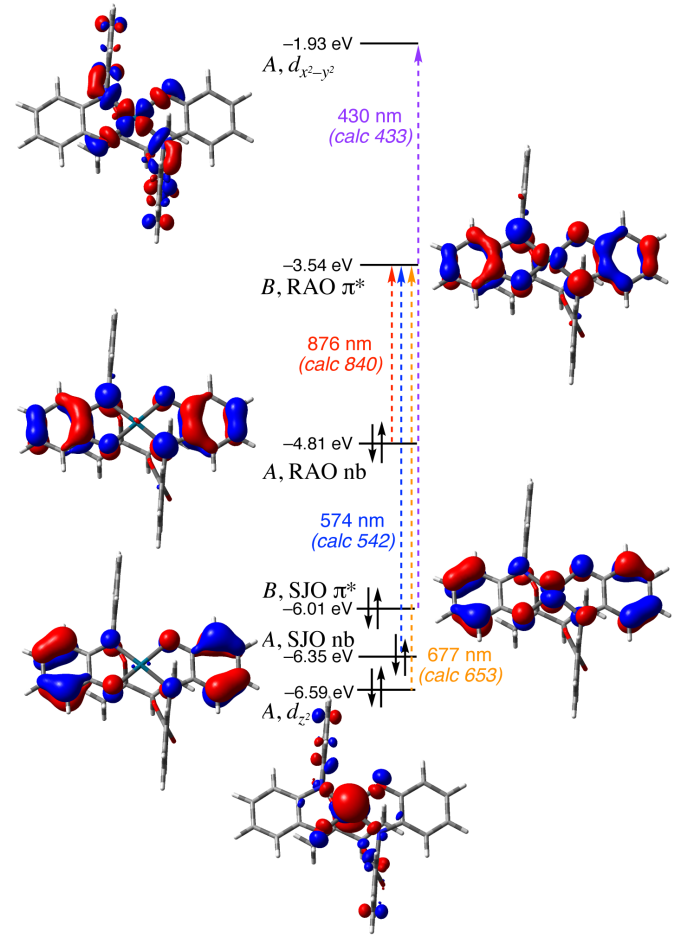

Fig. 7 MO diagram and assignment of optical spectrum of (*C*,*R*,*R*)-(Bdan)Pd. *A*-symmetry Kohn-Sham orbitals illustrated at bottom and left, *B*-symmetry orbitals at right.

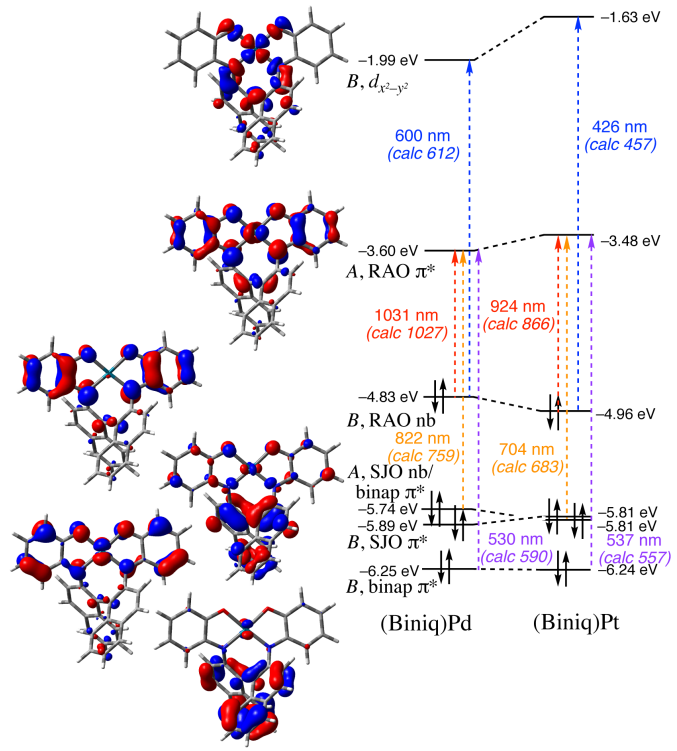

Fig. 8 MO diagram and assignment of optical spectrum of (*R*)-(Biniq)Pd (left) and (*R*)-(Biniq)Pt (right). Kohn-Sham orbitals illustrated for Pd, in the energy order of the Pd complex.

Synthesis of (*R*,*R*)-2,3-butanediyldianthranilate-bridged oxo bis-(amidophenoxide)osmium complexes. Because reactions of the biphenyl-bridged bis(aminophenol) ClipH_4 with osmium precursors affords only octahedral, oxo-free complexes, we did

not attempt preparation of (Biniq)OsO. In contrast, reaction of (*R*,*R*)-BdanH$_4$ with OsO(OCH$_2$CH$_2$O)$_2$ affords mixtures of the (*A*,*R*,*R*) and (*C*,*R*,*R*) diastereomers of (Bdan)OsO (eqn (6)). When the reaction is carried out in benzene at 80 °C, the (*A*,*R*,*R*) diastereomer is formed in 2.4:1 excess over the (*C*,*R*,*R*) diastereomer. Metalation at 115 °C in toluene also shows a preponderance of the (*A*,*R*,*R*) diastereomer at short reaction times (4:1 at 1 hr, while metalation is incomplete), but continued heating for 24 h results in essentially complete stereoselectivity in favor of the (*C*,*R*,*R*) isomer (> 30:1 dr). Pure (*C*,*R*,*R*)-(Bdan)OsO can be isolated from the reaction mixture at this point after filtration through silica gel and crystallization from methanol. The compound shows diamagnetic NMR spectra consistent with C_2 symmetry, and the coupling constants observed in the 2,3-butanediyl bridge (identical to those in (Bdan)Pd, Fig. S16) indicate that the bridge adopts a conformation with *anti* methyl groups. Other spectroscopic parameters (e.g., $\nu_{Os=O}$ = 916 cm^{-1}) closely match those observed for previously prepared oxoosmium bis(amidophenoxide) complexes.[20]

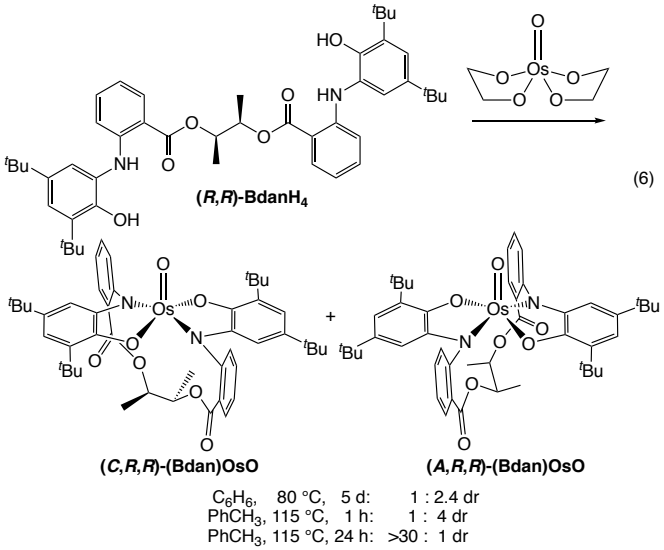

Crystallization of the isolated compound from methanol confirms its identity as the (*C*,*R*,*R*) diastereomer (Fig. 9), whose bridge conformation is similar to that of (*C*,*R*,*R*)-(Bdan)Pd. Crystallization from hexane of the mixture of diastereomers obtained from metalation in benzene at 80 °C results in cocrystallization of the (*C*,*R*,*R*) and (*A*,*R*,*R*) diastereomers in a 1:1 ratio (a quasiracemate). The molecular structure of the (*C*,*R*,*R*) isomer in this crystal is indistinguishable from that in the pure material, but the (*A*,*R*,*R*) isomer (Fig. 10) has a noticeably different conformation of the butanediyl dianthranilate bridge. The methyl groups remain *anti* (consistent with the similar appearance of its ^{1}H NMR signals), but the C2–C3 bond is now roughly aligned with the O–Os–O axis rather than the N–Os–N axis. Other structural features of the two compounds are very similar both to each other and to (Egan)OsO (Table 2).[20]

From the dependence of the ratio of diastereomers on the reaction conditions, it appears that (*C*,*R*,*R*)-(Bdan)OsO is the thermodynamically favored diastereomer. This is consistent with DFT calculations, which place it 2.3 kcal mol^{-1} lower in energy than the (*A*,*R*,*R*) isomer. The difference in energy may plausibly be attributed to a preference for the conformation in which the C2–C3 bond aligns with the N–Os–N axis, as seen in the solid-state structures of (*C*,*R*,*R*)-(Bdan)OsO and the ethylene-bridged analogue (Egan)OsO. This preference is reflected in the ^{1}H NMR spectrum of (Egan)OsO, which shows distinct *anti* and *gauche* couplings in the *AA'BB'* pattern of the CH$_2$CH$_2$ bridge (11.8 and 1.8 Hz, respectively, see Fig. S17). Were both conformers present to an appreciable extent, the coupling constants $J_{AA'}$ and $J_{BB'}$ would show a weighted average between *anti* and *gauche* values.

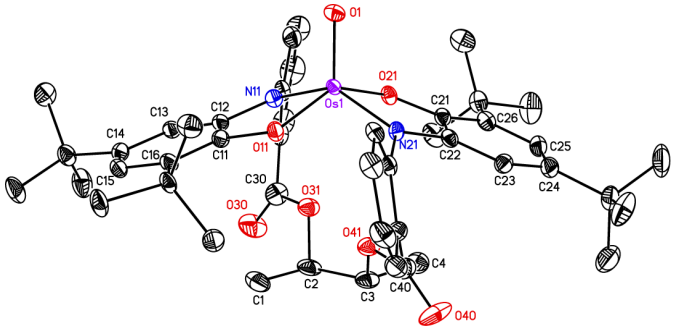

Fig. 9 Thermal ellipsoid plot of one molecule of (*C*,*R*,*R*)-(Bdan)OsO from the diastereomerically pure crystal. Hydrogen atoms are omitted for clarity.

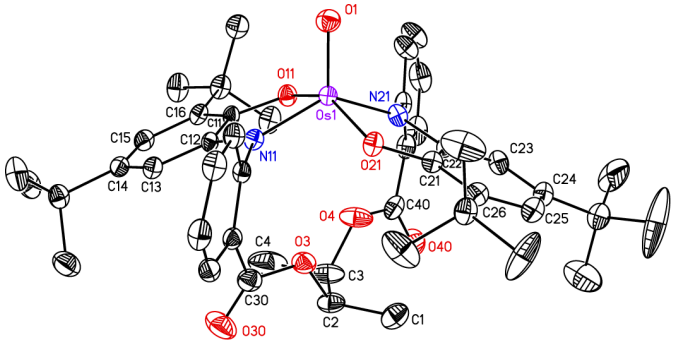

Fig. 10 Thermal ellipsoid plot of (*A*,*R*,*R*)-(Bdan)OsO from the quasiracemic crystal. Hydrogen atoms are omitted for clarity.

Optical and CD spectroscopy and electronic structure of the oxobis(iminoxolene)osmium chromophore. The UV-visible spectrum of (*C*,*R*,*R*)-(Bdan)OsO (Fig. 11) is, as expected, similar to previously reported oxobis(amidophenoxide) osmium complexes, especially (Egan)OsO.[20] In those complexes, the two lowest-energy transitions (in (Bdan)OsO, a weak shoulder at 579 nm and a peak at 444 nm) were assigned to transitions from the HOMO–1 (the *A*-symmetry RAO combination) to the two osmium-oxo π* orbitals. The difference in energy between the two bands is due to the difference in energy of the π* orbitals, with the higher-lying orbital being π* with respect to the *B*-symmetry RAO combination in addition to the oxo group. The difference in intensity is consistent with this assignment, as the intensity of optical transitions in trans bis-iminoxolene complexes arises principally from *B*→*A* or *A*→*B* transitions with ligand character in both orbitals. The higher-lying π* orbital has more ligand character and hence transitions to it have more intensity.

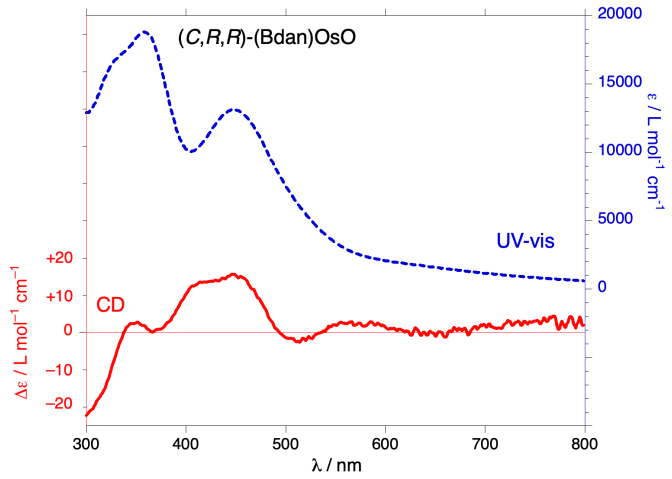

Fig. 11 Optical (blue dashed line, right axis) and circular dichroism (red solid line, left axis) spectra in CH_2Cl_2 of (*C*,*R*,*R*)-(Bdan)OsO.

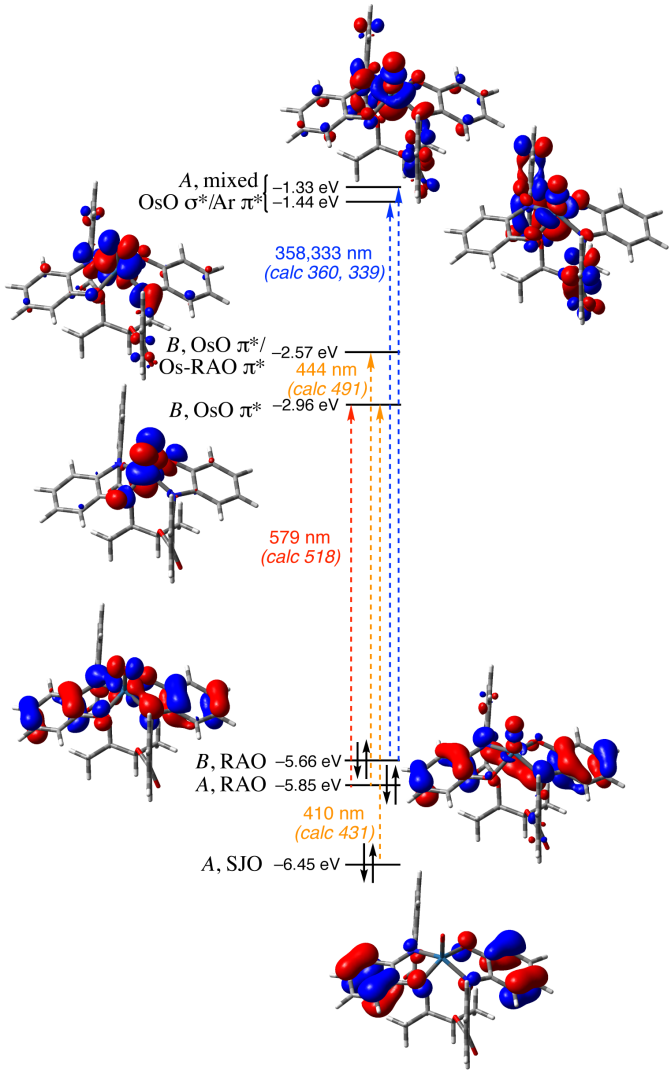

Fig. 12 MO diagram and assignment of optical spectrum of (*C*,*R*,*R*)-(Bdan)OsO. *B*-symmetry Kohn-Sham orbitals illustrated at left, *A*-symmetry orbitals at right.

The CD spectrum of (*C*,*R*,*R*)-(Bdan)OsO supports these assignments (Fig. 12), with the HOMO–1→LUMO transition calculated to have a weak CD signal and the HOMO–1 → LUMO+1 transition calculated to have a strong positive signal. The CD spectrum reveals a second band at 410 nm, assigned to a transition originating in the *A*-symmetry SJO combination. The high-energy band at ~350 nm, calculated to have a small CD signal, is clearly split. It is assigned to a transition from the *B*-symmetry HOMO to the *A*-symmetry Os-oxo σ* orbital, which is also π* with respect to the RAOs. The splitting of the band is due to mixing of the σ* orbital with the π* orbitals of the *N*-aryl groups.

Conclusions

Two distinct architectures of chiral bis(aminophenols) have been prepared in optically active form from commercially available materials. The first, (*R*)-BiniqH_4, is prepared in a single step from (*R*)-1,1′-binaphthyl-2,2′-diamine. This ligand, when metalated to give an approximately square planar geometry as in palladium and platinum bis(iminosemiquinone) complexes, has a C_2 axis in the approximate molecular plane. The geometry must be cis, and the *R* configuration of the biaryl backbone induces a *M* twist between the ligand planes. The second architecture is instantiated by the (*R*,*R*)-BdanH_4 ligand, prepared in two steps from (*R*,*R*)-2,3-butanediol via its anthranilate diester. Here binding in a roughly square array, as in four-coordinate (Bdan)Pd or five-coordinate (Bdan)OsO, takes place with a trans arrangement of ligands and with the ligand C_2 axis perpendicular to the ligand plane. Thus, the 2,3-butanediyldianthranilate moiety forms a "strap" that blocks one face of the ligand plane. In contrast to (*R*)-Biniq, which can only form one possible stereoisomer on metalation, the prochiral nature of the trans-MN_2O_2 arrangement results in two possible diastereomers of the metal complex, depending on which enantioface is blocked by the chiral strap. Palladium is metalated stereospecifically, with only the (*C*,*R*,*R*) isomer being observed. Kinetically, reaction of (*R*,*R*)-BdanH_2 with $OsO(OCH_2CH_2O)_2$ gives mixtures of diastereomers, but prolonged reaction at high temperature gives selectively the (*C*,*R*,*R*) isomer as well. For both sets of chromophores, circular dichroism spectroscopy gives an additional dimension to the optical spectra, allowing greater insight into the details of bonding in the two types of complex.

Conflicts of interest

There are no conflicts to declare.

Acknowledgements

This work was supported by the US National Science Foundation (CHE-1955933). H. C. acknowledges support from a Notre Dame College of Science Summer Undergraduate Research Fellowship. J. J. acknowledges support through a MERIT fellowship (US Dept. of Education grant number P200A210048) and from the University of Notre Dame (College of Engineering and the Graduate School). We thank Dr. Allen G. Oliver for his assistance with X-ray crystallography, and Dr. Giselle Jacobson

for her assistance with the CD spectroscopy of (*C*,*R*,*R*)-(Bdan)OsO.

Notes and references

1 D. L. J. Broere, R. Plessius and J. I. van der Vlugt, *Chem. Soc. Rev.*, 2015, **44**, 6886-6915.
2 R. F. Munhá, R. A. Zarkesh and A. F. Heyduk, *Dalton Trans.*, 2013, **42**, 3751-3766.
3 M. R. Haneline and A. F. Heyduk, *J. Am. Chem. Soc.*, 2006, **128**, 8410-8411.
4 D. L. J. Broere, B. de Bruin, J. N. H. Reek, M. Lutz, S. Dechert and J. I. van der Vlugt, *J. Am. Chem. Soc.*, 2014, **136**, 11574-11577.
5 J. Gianino and S. N. Brown, *Dalton Trans.*, 2020, **49**, 7015-7027.
6 T. H. Do and S. N. Brown, *Inorg. Chem.*, 2022, **61**, 5547-5562.
7 A. N. Erickson, J. Gianino, S. J. Markovitz and S. N. Brown, *Inorg. Chem.*, 2021, **60**, 4004-4014.
8 T. Marshall-Roth, S. C. Liebscher, K. Rickert, N. J. Seewald, A. G. Oliver and S. N. Brown, *Chem. Commun.*, 2012, **48**, 7826-7828.
9 P. Chaudhuri, M. Hess, J. Müller, K. Hildenbrand, E. Bill, T. Weyhermüller and K. Wieghardt, *J. Am. Chem. Soc.*, 1999, **121**, 9599-9610.
10 K. S. Min, T. Weyhermüller, E. Bothe and K. Wieghardt, *Inorg. Chem.*, 2004, **43**, 2922-2931.
11 (a) R. Metzinger, S. Demeshko and C. Limberg, *Chem. Eur. J.*, 2014, **20**, 4721-4735. (b) M. K. Mondal, A. K. Biswas, B. Ganguly and C. Mukherjee, *Dalton Trans.*, 2015, **44**, 9375-9381.
12 D. D. Swanson, K. M. Conner and S. N. Brown, *Dalton Trans.*, 2017, **46**, 9049-9057.
13 T. Marshall-Roth and S. N. Brown, *Dalton Trans.*, 2015, **44**, 677-685.
14 P. Chaudhuri, M. Hess, J. Müller, K. Hildenbrand, E. Bill, T. Weyhermüller and K. Wieghardt, *J. Am. Chem. Soc.*, 1999, **121**, 9599-9610.
15 A. L. Smith, K. I. Hardcastle and J. D. Soper, *J. Am. Chem. Soc.*, 2010, **132**, 14358-14360.
16 Y. Ren, K. Cheaib, J. Jacquet, H. Vezin, L. Fensterbank, M. Orio, S. Blanchard and M. Desage-El Murr, *Chem. Eur. J.*, 2018, **24**, 5086-5090.
17 J. Autschbach, F. E. Jorge and T. Ziegler, *Inorg. Chem.*, 2003, **42**, 2867-2877.
18 C. Mukherjee, T. Weyhermüller, E. Bothe and P. Chaudhuri, *Inorg. Chem.*, 2008, **47**, 11620-11632.
19 K. M. Conner, A. L. Perugini, M. Malabute and S. N. Brown, *Inorg. Chem.* 2018, **57**, 3272-3286.
20 J. Gianino, A. N. Erickson, S. J. Markovitz and S. N. Brown, *Dalton Trans.*, 2020, **49**, 8504-8515.
21 G. Bott, L. D. Field and S. Sternhell, *J. Am. Chem. Soc.*, 1980, **102**, 5618-5626.
22 P. N. O'Shaughnessy, P. D. Knight, C. Morton, K. M. Gillespie and P. Scott, *Chem. Commun.*, 2003, 1770-1771.
23 P. D. Knight, I. Munslow, P. N. O'Shaughnessy and P. Scott, *Chem. Commun.*, 2004, 894-895.
24 P. N. O'Shaughnessy, K. M. Gillespie, P. D. Knight, I. J. Munslow and P. Scott, *Dalton Trans.*, 2004, 2251-2256.
25 (a) K. M. Gillespie, C. J. Sanders, P. O'Shaughnessy, I. Westmoreland, C. P. Thickitt and P. Scott, *J. Org. Chem.*, 2002, **67**, 3450-3458. (b) M. C. Wood, D. C. Leitch, C. S. Yeung, J. A. Kozak and L. L. Schafer, *Angew. Chem. Int. Ed.*, 2007, **46**, 354-358, as corrected in *Angew. Chem. Int. Ed.*, 2009, **48**, 6937.
26 Y. Ren, J. Forté, K. Cheaib, N. Vanthuyne, L. Fensterbank, H. Vezin, M. Orio, S. Blanchard and M. Desage-El Murr, *iScience*, 2020, **23**, 100955.
27 R. J. Collin, J. Jones and W. P. Griffith, *J. Chem. Soc., Dalton Trans.*, 1974, 1094-1097.
28 N. G. Connelly and W. E. Geiger, *Chem. Rev.*, 1996, **96**, 877-910.
29 D. Lionetti, A. J. Medvecz, V. Ugrinova, M. Quiroz-Guzman, B. C. Noll and S. N. Brown, *Inorg. Chem.*, 2010, **49**, 4687-4697.
30 D. C. Harris, *J. Chem. Educ.*, 1998, **75**, 119-121.
31 R. de Levie, *J. Chem. Educ.*, 1999, **76**, 1594-1598.
32 M. J. Frisch, G. W. Trucks, H. B. Schlegel, G. E. Scuseria, M. A. Robb, J. R. Cheeseman, G. Scalmani, V. Barone, G. A. Petersson, H. Nakatsuji, X. Li, M. Caricato, A. V. Marenich, J. Bloino, B. G. Janesko, R. Gomperts, B. Mennucci, H. P. Hratchian, J. V. Ortiz, A. F. Izmaylov, J. L. Sonnenberg, D. Williams-Young, F. Ding, F. Lipparini, F. Egidi, J. Goings, B. Peng, A. Petrone, T. Henderson, D. Ranasinghe, V. G. Zakrzewski, J. Gao, N. Rega, G. Zheng, W. Liang, M. Hada, M. Ehara, K. Toyota, R. Fukuda, J. Hasegawa, M. Ishida, T. Nakajima, Y. Honda, O. Kitao, H. Nakai, T. Vreven, K. Throssell, J. A. Montgomery Jr., J. E. Peralta, F. Ogliaro, M. J. Bearpark, J. J. Heyd, E. N. Brothers, K. N. Kudin, V. N. Staroverov, T. A. Keith, R. Kobayashi, J. Normand, K. Raghavachari, A. P. Rendell, J. C. Burant, S. S. Iyengar, J. Tomasi, M. Cossi, J. M. Millam, M. Klene, C. Adamo, R. Cammi, J. W. Ochterski, R. L. Martin, K. Morokuma, O. Farkas, J. B. Foresman and D. J. Fox, Gaussian 16, Revision B.01, Gaussian, Inc., Wallingford CT, 2016.
33 G. M. Sheldrick, *Acta Cryst. A*, 2008, **A64**, 112-122.
34 *International Tables for Crystallography*, ed. A. J. C. Wilson, Kluwer Academic Publishers: Dordrecht, The Netherlands, 1992, Vol C.
35 S. N. Brown, *Inorg. Chem.*, 2012, **51**, 1251-1260.
36 G. V. Gridunova, N. G. Furmanova, Y. T. Struchkov, Z. I. Ezhkova, L. P. Grigoryeva and B. A. Chayanov, *Kristallografiya*, 1982, **27**, 267-272.
37 M. D. Jones, F. A. Almeida Paz, J. E. Davies and B. F. G. Johnson, *Acta Cryst.*, 2003, **E59**, o910-o912.
38 M. Nishizaka, T. Mori and Y. Inoue, *J. Phys. Chem. A*, 2011, **115**, 5488-5495.
39 R. P. Staiger and E. B. Miller, *J. Org. Chem.*, 1959, **24**, 1214-1219.
40 N. G. Connelly, T. Damhus, R. M. Hartshorn and A. T. Hutton, *Nomenclature of Inorganic Chemistry IUPAC Recommendations 2005*, RSC Publishing: Cambridge, UK, 2005.
41 (a) P. Chaudhuri, C. N. Verani, E. Bill, E. Bothe, T. Weyhermüller and K. Wieghardt, *J. Am. Chem. Soc.*, 2001, **123**, 2213-2223. (b) X. Sun, H. Chun, K. Hildenbrand, E. Bothe, T. Weyhermüller, F. Neese and K. Wieghardt, *Inorg. Chem.*, 2002, **41**, 4295-4303.
42 (a) M. O. Talismanova, I. G. Fomina, A. A. Sidorov, G. G. Aleksandrov, N. T. Berberova, A. O. Okhlobystin, E. V. Shinkar, I. F. Golovaneva, I. L. Eremenko and I. I. Moiseev, *Russ. Chem. Bull.*, 2003, **52**, 2701-2706. (b) D. Herebian, E. Bothe, F. Neese, T. Weyhermüller and K. Wieghardt, *J. Am. Chem. Soc.*, 2003, **125**, 9116-9128.